ELSEVIER

Journal of South American Earth Sciences 25 (2008) 359–376

Journal of
South American
Earth Sciences

www.elsevier.com/locate/jsames

Morphology and composition of gold in a lateritic profile, Fazenda Pison "Garimpo", Amazon, Brazil

J.H. Larizzatti [a,*], S.M.B. Oliveira [b], C.R.M. Butt [c]

[a] *CPRM/Geological Survey of Brazil, Av. Pasteur, 404, Rio de Janeiro, RJ 22290-240, Brazil*
[b] *Universidade de São Paulo, Rua do Lago, 562, São Paulo, SP 05508-900, Brazil*
[c] *CRC LEME, CSIRO Exploration and Mining, PO Box 1130, Bentley, WA 6102, Australia*

Abstract

This study describes the morphological evolution of gold grains in a lateritic weathering profile in an equatorial rainforest climate. Primary sources of gold are quartz veins associated with shallow granophyric intrusion. Gold grains were found in fresh ore, saprolite, transition zones, ferruginous duricrust, red latosol, and yellow latosol. Irregularly shaped grains predominate, with smaller proportions of dendritic and prismatic forms. Gold grains are weathered in the uppermost 10 m of the regolith. Mean gold grain size is maximum in the duricrust (>125 μm) and decreases progressively upward into the yellow latosol (<90 μm). Voids and corrosion pits appear on grain surfaces, and progressive rounding is observed from the bottom of the profile to the top. Gold grains can be classified as either homogeneous or zoned with respect to their chemical composition. Homogeneous grains contain 2–15% Ag (mean 8.3%). Zoned grains have more variable Ag contents; grain cores have means of approximately 10% or 23% Ag, with Ag-poor zones of approximately 3.7% Ag along internal discontinuities and/or outer rims. Formation of Ag-poor rims is due to preferential depletion of silver. Processes responsible for duricrust formation may preserve some grains as large aggregates, but subsequent transformation into latosol further modifies them.

Keywords: Gold grains; Morphology; Composition; Weathering; Laterites; Amazon

1. Introduction

The supergene mobility of gold in weathering profiles has been well documented in different parts of the world (e.g., Boyle, 1979; Mann, 1984; Wilson, 1984; Webster and Mann, 1984; Davy and El-Ansary, 1986; Michel, 1987; Freyssinet and Butt, 1988; Colin et al., 1989a,b; Freyssinet et al., 1987; Grimm and Friedrich, 1990; Colin and Vieillard, 1991; de Oliveira and Campos, 1991; Santosh and Omana, 1991; Vasconcelos and Kyle, 1991; Edou Minko et al., 1992; Bowell, 1992; Freyssinet, 1993; Lawrance and Griffin, 1994; Sergeev et al., 1994; Porto and Hale, 1996; de Oliveira and de Oliveira, 2000). Evidence of gold dissolution includes the decreasing size of gold grains from the bottom to the top of weathering profiles and the presence of corrosion features on the surface of primary crystals (Colin et al., 1989a,b; Colin and Vieillard, 1991; Porto and Hale, 1996). Gold precipitation is demonstrated by the formation of secondary crystals of high fineness and characteristic morphology (Angélica et al., 1995; Freyssinet et al., 1987; Grimm and Friedrich, 1990; Bowell, 1992; Lawrance and Griffin, 1994) and gold nuggets enclosing neoformed goethite (Machairas, 1963; Wilson, 1984; Vasconcelos and Kyle, 1991; Santosh and Omana, 1991; de Oliveira and Campos, 1991; Zang and Fyfe, 1993). Further data supporting gold mobility in the supergene environment include elevated gold concentrations in stream waters draining auriferous zones (Benedetti and Boulège, 1991; Andrade et al., 1991) and grain growth in stream sediments (Eyles, 1990; Groen et al., 1990; Craw, 1992; Youngson and Craw, 1995; McCready et al., 2003). The objective of this study is to provide some data on the morphology and composition of gold in a well-preserved

* Corresponding author. Tel.: +55 21 2542 0586; fax: +55 21 2295 4292.
E-mail address: joao@rj.cprm.gov.br (J.H. Larizzatti).

0895-9811/$ - see front matter © 2007 Elsevier Ltd. All rights reserved.
doi:10.1016/j.jsames.2007.06.002

lateritic profile derived from a quartz (+pyrite) vein system in the Tapajós region.

2. Description of the area

2.1. Climate

The Fazenda Pison "Garimpo" (artisinal mine working) is located in northern Brazil, near the Tapajós River, about 600 km SE of Manaus, Amazonas State (Fig. 1). The area has a warm to hot humid rainforest climate, with mean minimum temperature of 17 °C (February), mean maximum temperature of 38 °C (July), and mean annual rainfall of 2750 mm. The relief is of the "half-orange" type, at elevations of 140–200 m above sea level.

2.2. Geology

The Garimpo is located in the Tapajós Province (Almeida et al., 1981), Tapajós Mineral Province (Santos et al., 2001). Felsic volcanic rocks (Iriri Group, Andrade et al., 1978; CPRM, 1999) occur where shallow granitic intrusions (Maloquinha Intrusive Suite; Santos et al., 1997) are emplaced along brittle shear zones.

Primary mineralization at Fazenda Pison follows a third-order brittle shear zone (N20E) hosted by fine granophyric rock. The mineralized veins are dislocated by late sinistral brittle faults (ENE). A hydrothermal alteration envelope follows the host structure and is expressed by mineralogical zoning around the mineralized quartz veins:

Central zone: gold, quartz, white mica, epidote, pyrite, hematite, and magnetite;

Intermediate zone: minor gold, quartz, white mica, epidote, fluorite, and magnetite; and

Distal zone: minor gold, quartz, white mica, chlorite, and magnetite.

At the top of the saprolite, a meter-wide stockwork zone is visible adjacent to the quartz veins. The lode is subvertical, with an overall width, including the alteration zone, of 20 m. Rounded, decimeter-sized, quartz-rich zones can be observed within the stockwork zone.

The Amazon region is characterized by a deep lateritic regolith, and at Fazenda Pison, the weathering profile is 20–30 m deep. The studied profile is located in a hillslope. Six main units can be recognized in a fully preserved lateritic profile (Fig. 2):

1. Saprolite: >20 m thick, light red, with well-preserved primary fabrics and structures. Primary white micas can be recognized, but feldspars, chlorite, fluorite, and sulphides cannot (boxwork texture is present). Quartz, white

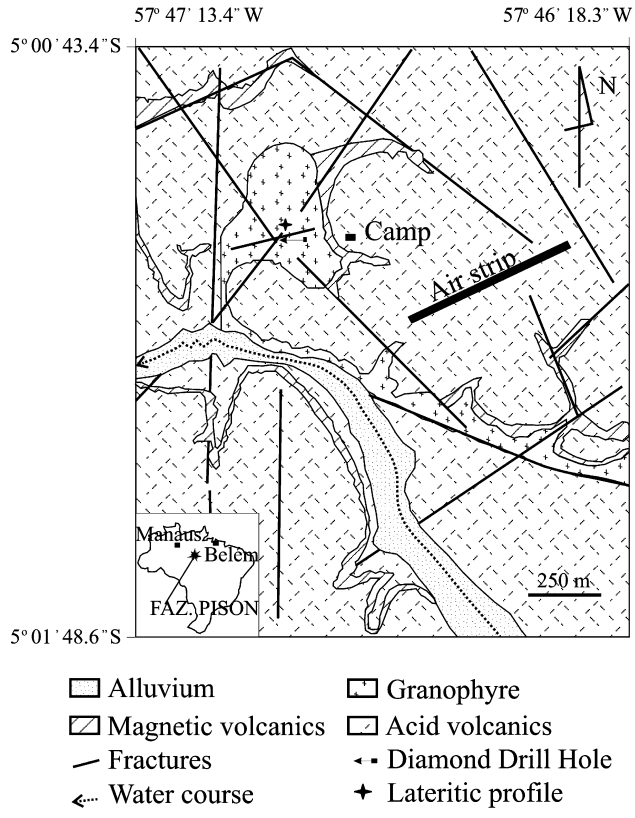

Fig. 1. Area localization and geological sketch modified from RTDM (1995).

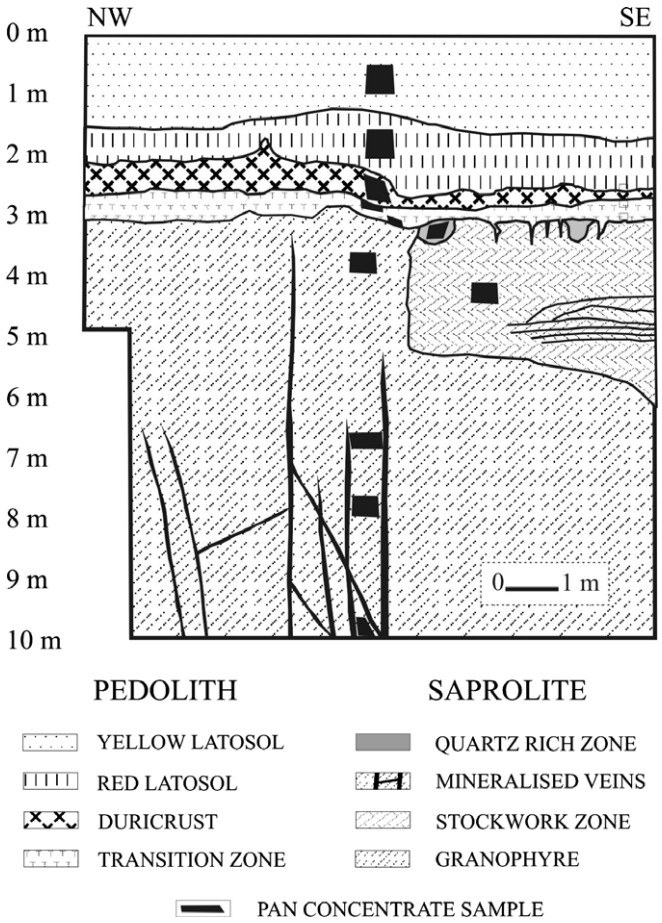

Fig. 2. Weathering profile and sampling sites.

mica, kaolinite, and hematite (+little goethite) are the most abundant minerals present. The contact with lower transition zone is gradational and centimetric; saprolite fragments decrease in size and are immersed in a clay-rich matrix.

2. Lower transition zone: <0.5 m thick, red, with numerous weathered lithic fragments that preserve primary rock fabrics immersed in a kaolinite-rich matrix containing iron oxi-hydroxides (hematite/goethite). From saprolite to the lower transition zone, there is an increase in quartz content, decrease in white-mica content, and no change in iron oxi-hydroxides and kaolinite contents. The transition to the upper transition zone is gradational; iron-rich pisoliths are formed and increase in size, forming nodules in the top of the horizon.
3. Upper transition zone: 0.2 m thick, with ferruginous pisoliths and nodules embedded in a ferruginous kaolinite matrix. No primary fabric can be observed in this material. From lower to the upper transition zone, quartz and white-mica contents decrease, and an important increase in iron oxi-hydroxides contents (specially hematite) and kaolinite can be noted. The transition to duricrust is gradational; iron-rich nodules become bigger and more numerous and form an indurated duricrust.
4. Duricrust: (discontinuous ferruginous horizon) of variable thickness (usually <1 m), with a high concentration of hematite. From upper transition zone to duricrust, an important decrease in quartz content and important increase in hematite/goethite and kaolinite contents occur. Contact with red latosol is sharp, but at the base, it is possible to observe iron-rich pisoliths with yellow cortexes immersed in the clay-rich matrix.
5. Red latosol: clay-rich matrix (minor Fe) with nodules and pisoliths derived from the duricrust. Thickness varies from less than 1 m at the base of slopes to 6 m on hill crests. From duricrust to red latosol occurs an increase in quartz and kaolinite contents and important decrease in iron oxi-hydroxides (especially hematite). The transition to yellow latosol is gradational; at the top horizon, iron-rich pisoliths are not observed.
6. Yellow latosol: similar to red latosol, with lower contents of iron oxi-hydroxides. From red to yellow latosol, minor variations in quartz, kaolinite, and iron oxi-hydroxides contents are observed. At the top of this horizon rests a centimetric layer of a dark-brown organic matter-rich material.

3. Methods

A schematic cross-section of the pit at the Fazenda Pison Garimpo and the sampling sites are shown in Fig. 2. Samples were collected from the mineralized zone and different horizons of the regolith developed above it, as follows: One sample (0.94 kg) of primary ore was collected from a diamond drill core and jaw-crushed to 5 mm, then ground in a disc mill to 1.5 mm. It is not shown in Figs. 2 and 3.

Bulk samples of 50 kg each where taken from the regolith as follows: (1) six samples of saprolite, specifically, four samples from granophyre saprolite, at 10, 8, 7, and 4 m; one sample from the stockwork zone; and one sample from a quartz-rich zone; (2) two samples from the transition zone, one from the upper and one from the lower; (3)

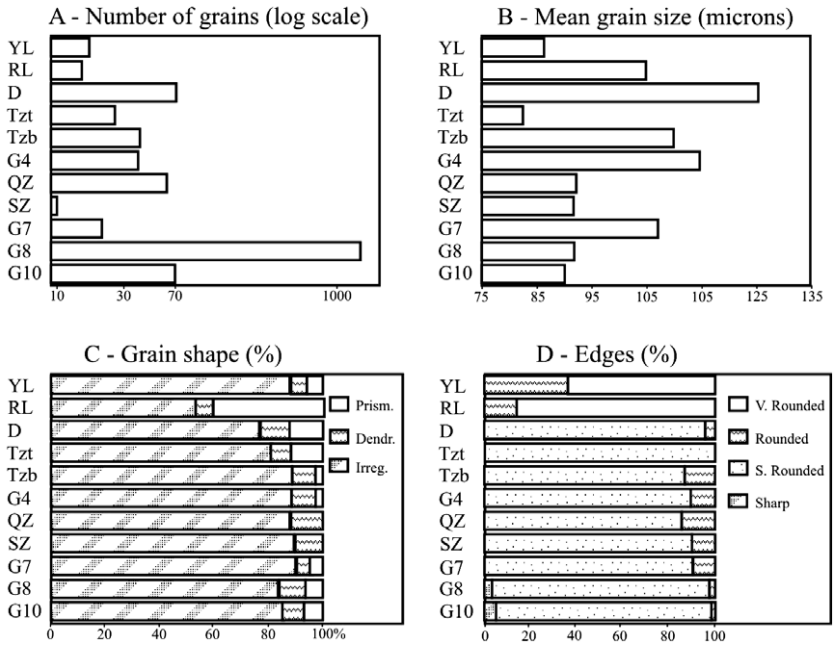

Fig. 3. Characteristics of gold particles according to regolith unit (YL, yellow latosol; RL, red latosol; D, duricrust; TZt, transition zone-top; TZb, transition zone-base; G4, saprolite, granophyre 4 m deep; QZ, saprolite, quartz-rich zone; SZ, saprolite stockwork zone; G7, saprolite; granophyre 7 m deep; G8, saprolite, granophyre 8 m deep; G10, saprolite, granophyre 10 m deep). (A) Number of particles; (B) particle size (μm); (C) particle shape (%), where Prism, prismatic; Dendr., dendritic; Irreg., irregular; and (D) edge roundness (%), where V. Rounded, very rounded; S. Rounded, sub-rounded.

one sample from the duricrust; (4) one sample from the red latosol; and (5) one sample from the yellow latosol.

Samples were processed as follows:

1. Field: samples collected at the lateritic profile were panned and dried in the field. Samples from primary ore and duricrust were hand crushed before panning.
2. Laboratory preparation: samples were oven dried at 70 °C. Magnetic minerals were separated using a hand magnet and Frantz magnetic separator. Heavy minerals were separated using heavy liquid (methylene iodide). Gold grains were handpicked under a binocular microscope.
3. Optical examination: gold grains were mounted on glass slides with double-sided adhesive tape and examined using a binocular microscope. Grains were classified according to their morphology; some were selected for further study.
4. Scanning electron microscopy (SEM): grain morphology was examined by SEM, and the Ag content was determined semi-quantitatively using an energy dispersive spectrometer. Instruments used were a JEOL JSM-6400 and Electroscan ESEM(S) E-3, Centre of Microscopy and Microanalysis, University of Western Australia (CMM/UWA), operating at 20–30 kV accelerating voltage, 3×10^{-12} A primary beam current, and 9–20 mm working distance.
5. Polished section: selected grains were examined in polished section by SEM.
6. Electron microprobe (EPMA): fifty-four gold grains (polished sections) were analysed for Au, Ag, As, Bi, Cu, Fe, Hg, Pt, Sb, and Zn using a JEOL 6400 instrument at CMM/UWA. Operating conditions and detection limits are given in Table 1.

Approximately 1850 gold grains were examined by optical microscopy, 300 representative gold grains by SEM, and 54 grains by EPMA (Table 2).

The data discussed in this paper refer only to the grains recovered and examined by these procedures. A high proportion of grains smaller than 10 μm were lost, with moderate losses of those between 10 and 20 μm.

4. Results

4.1. Size and morphology of gold grains

4.1.1. Classification

The number and morphological characteristics of gold grains in the different regolith horizons are summarized in Fig. 3. The grains were classified in terms of location of regolith material (Fig. 2); size, as $(\text{length} \times \text{width})^{1/2}$ (Fig. 3B); habit, as to prismatic, when gold grains show similar length in three dimensions and smooth/near smooth faces (e.g., Figs. 4B, 7E, and 8B) or dendritic, when one dimension is much more developed than the other two (e.g., Figs. 6A, B, and 7F) or irregular, when gold grains do not show smooth faces or one distinctive dimension (e.g., Figs. 5A, B, E, F, 7A–D, and 8A, E, F); and edges, in terms of whether they are sharp (e.g., Figs. 4A, B, and 5A), sub-

Table 1
Operating conditions and detection limits for EMPA

Instrument conditions						
Accelerating voltage = 25 kV			Primary beam current = 2.8×10^{-12} A			
	Au	Ag	As	Bi	Cu	Fe
Detection limit (wt%)	0.131	0.033	0.031	0.092	0.018	0.017
Counting time (s)	25	25	25	25	25	25

Table 2
Number of gold grains analysed and number of analyses according to sampling medium (EMPA)

Sampling medium	Homogeneous grains		Zoned grains		
	Number of grains	Number of analyses	Number of grains	Number of analyses – core	Number of analyses – rim
Yellow latosol	3	11	7	11	9
Red latosol	4	15	1	1	2
Duricrust	6	21	8	38	20
Transition zone	None	None	5	19	4
Stockwork	None	None	5	10	7
Granophyre	None	None	9	19	14
Fresh ore	4	9	2	2	2

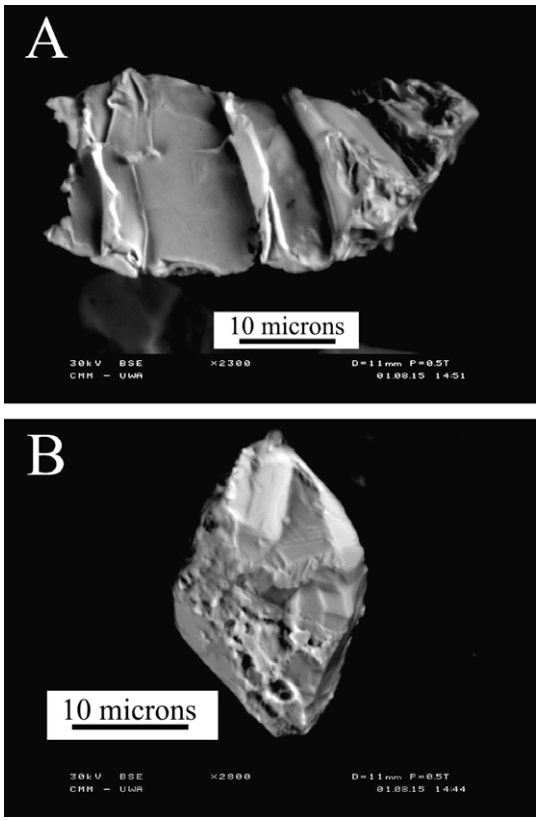

Fig. 4. Backscattered electron images (SEM) of primary gold grains.

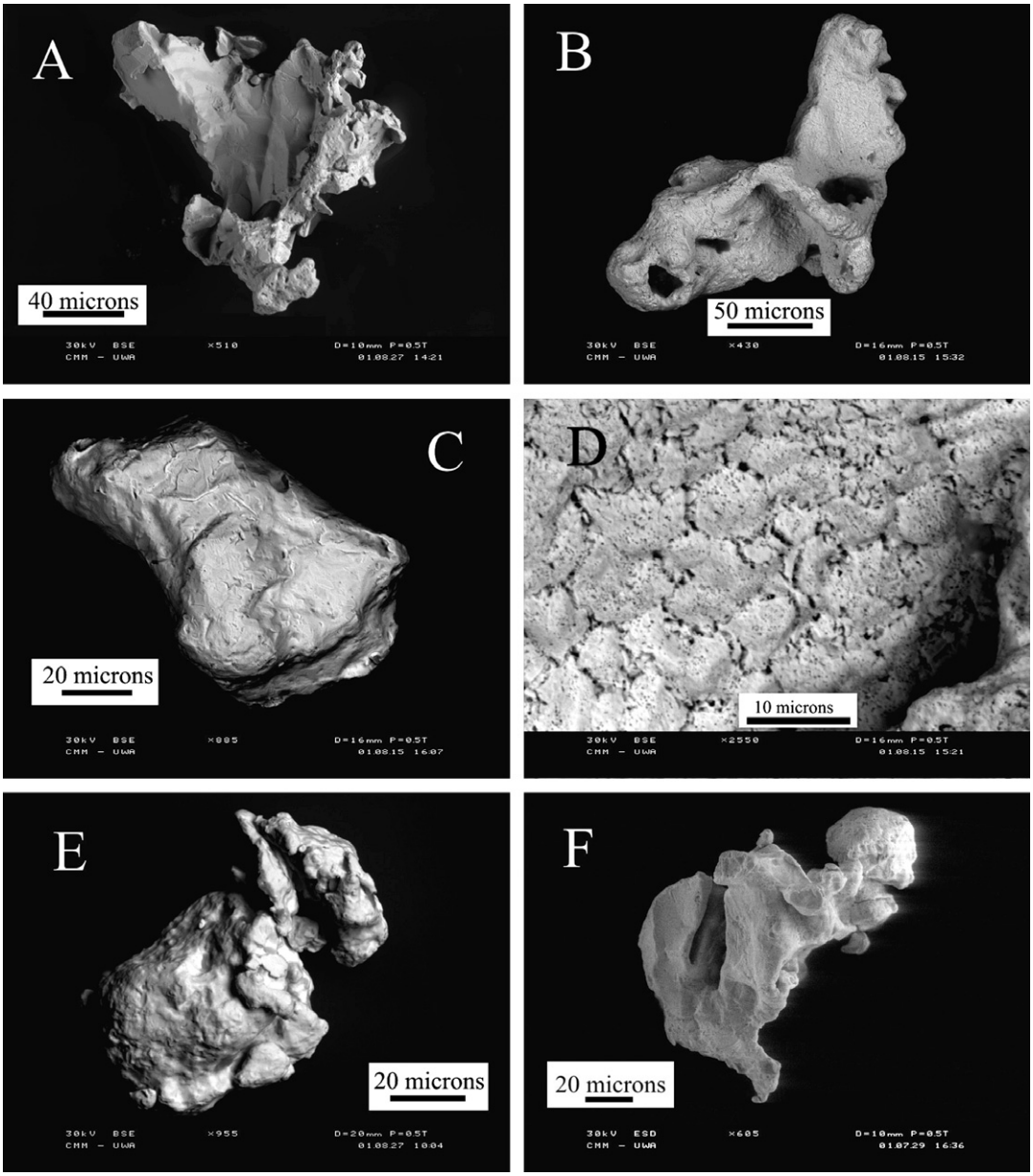

Fig. 5. Backscattered electron images (SEM) of gold grains recovered from saprolite. (A–D) Granophyre; (E) stockwork zone; and (F) quartz-rich zone.

rounded (e.g., Figs. 5C, E, F, and 6A), rounded (e.g., Figs. 5B and 6B), or very rounded (e.g., Fig. 8A and F).

4.1.2. Gold in primary mineralization

Primary gold is associated with pyritic quartz veins. Only 12 gold grains were recovered from the fresh ore, with a mean size of 56 μm. All grains are xenomorphic, with very smooth faces that show the impression of the surrounding quartz. There are two habits: irregular (Fig. 4A) and prismatic (Fig. 4B).

4.2. Saprolite

Grains separated from saprolite are shown in Fig. 5. The gold distribution in the granophyre saprolite is highly variable, as reflected by the number of grains recovered at different horizons (Fig. 3). The mean grain size is 92 μm ($\sigma = 46$). The majority of grains (Fig. 3C) are irregular in shape (83%), with about 10% of the grains dendritic and the remainder (7%) prismatic. Most grains have slightly rounded edges (94%), with the remainder strongly rounded or sharp.

More than 90% of the grains recovered from both stockwork zones and quartz-rich zone are irregular (Fig. 5E and F); the remainder are dendritic. Most grains from quartz-rich and stockwork zones show subrounded edges (85% and 92%, respectively), and the rest show rounded edges. Corrosion pits occur on most grains observed in the saprolite materials (Fig. 5A–F). Some grains show scratches (tool marks).

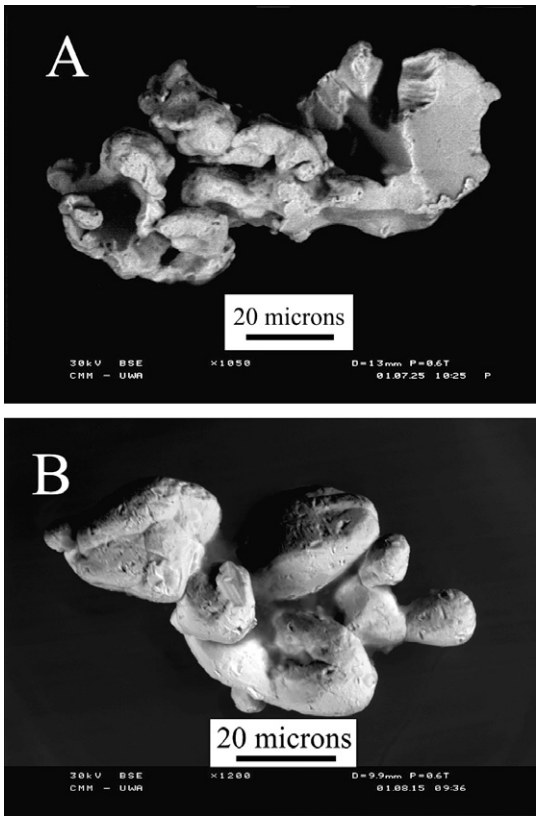

Fig. 6. Backscattered electron images (SEM) of gold grains recovered from transition zone. (A) Bottom of transition zone showing subrounded edges; (B) top of transition zone showing rounded edges.

4.3. Transition zone

Mean grain size is 108 μm ($\sigma = 76$) at the base and 81 μm ($\sigma = 23$) at the top of transition zone. Most grains from the transition zone are irregular (86%), and the rest are dendritic (8%) or prismatic (6%). There are more prismatic grains (12%) in the upper part of the zone than all underlying horizons. Edges and faces of grains are corroded and pitted (Fig. 6A and B). Some grains show scratches (tool marks) and folded rims.

4.4. Duricrust

Gold grains in the duricrust have the greatest mean size (124 μm, $\sigma = 72$; Fig. 3B). Nearly 80% of the grains are irregular (Figs. 3C and 7A–D), with nearly equal proportions of prismatic (Figs. 3C and 7E) and dendritic (Figs. 3C and 7F). Most grains have slightly rounded edges (96%) and numerous corrosion pits; some grains show scratches.

4.5. Latosol

In the red latosol, only 53% of the grains are irregular in habit; some 40% are prismatic, a much higher proportion than all underlying horizons, including the duricrust and upper transition zone; and the remainder are dendritic (Fig. 3C). Nearly 90% of the grains have very rounded edges, all show numerous corrosion pits (Figs. 3D and 8A, B), and the mean grain size (105 μm, $\sigma = 63$; Fig. 3B) is smaller than the underlying duricrust.

In the yellow latosol (Figs. 3C, 8C–F), the proportion of prismatic grains is approximately 6%, similar to that in the saprolite; most grains (88%) are irregular, and 6% are dendritic. The mean grain size is less than in the red latosol (86 μm, $\sigma = 28$). Most grains (65%) have very rounded edges with well-developed corrosion pits; nevertheless, it is possible to recognize the primary habit in many of the gold particles.

The progressive decrease of mean grain size from the duricrust to the yellow latosol, together with the increasing number of corrosion pits and degree of rounding, implies dissolution of gold. Gold is preferably dissolved from prominent parts of grains, and dissolution seems more active on dendritic and irregular grains than prismatic grains. Some grains recovered from both latosols show tool marks.

4.6. Chemical composition of gold grains

Chemical analysis of 54 gold particles was performed by EPMA (Tables 1–4). Only Au, Ag, and Cu are present in detectable amount in most grains; some also contain As, Bi, and Fe. Silver is the only element, other than gold, present in high concentrations. According to the silver distribution, there are two groups of gold grains: homogeneous and zoned (Fig. 9). The 17 analysed homogeneous grains (56 analyses) show a similar grey hue throughout the hole-polished section under SEM backscattered mode (Fig. 9A) and have Ag contents of 2.40–17.34% (mean 8.28%; Tables 3 and 4). The 37 analysed zoned grains (54 rim and 104 core analyses) show variable silver content throughout the polished section under SEM backscattered mode (Fig. 9B), lower silver contents in the outer rims, and internal discontinuities (0.02–14.09%, mean 3.64% Ag) compared with the cores (3.84–31.10%, mean 17.30% Ag; Tables 3 and 4). These internal variations are evident using SEM backscatter imaging and can be quantified by EPMA analysis. Some homogeneous and zoned grains show compositional variation within a single grain, core, or rim. In zoned grains, the contact between grain cores and silver-poor rims is commonly sharp. Zoned gold grains from the fresh ore do not show silver-poor rims; they show internal variations in Au and Ag contents that cannot be characterized as rims or cores, and they were not studied together with regolith zoned gold grains.

4.6.1. Homogeneous grains

Homogeneous gold grains were recovered from primary mineralization (fresh ore), duricrust, and latosols. The compositions of homogeneous particles vary between 82.25% and 98.20% Au and 2.40% and 17.34% Ag

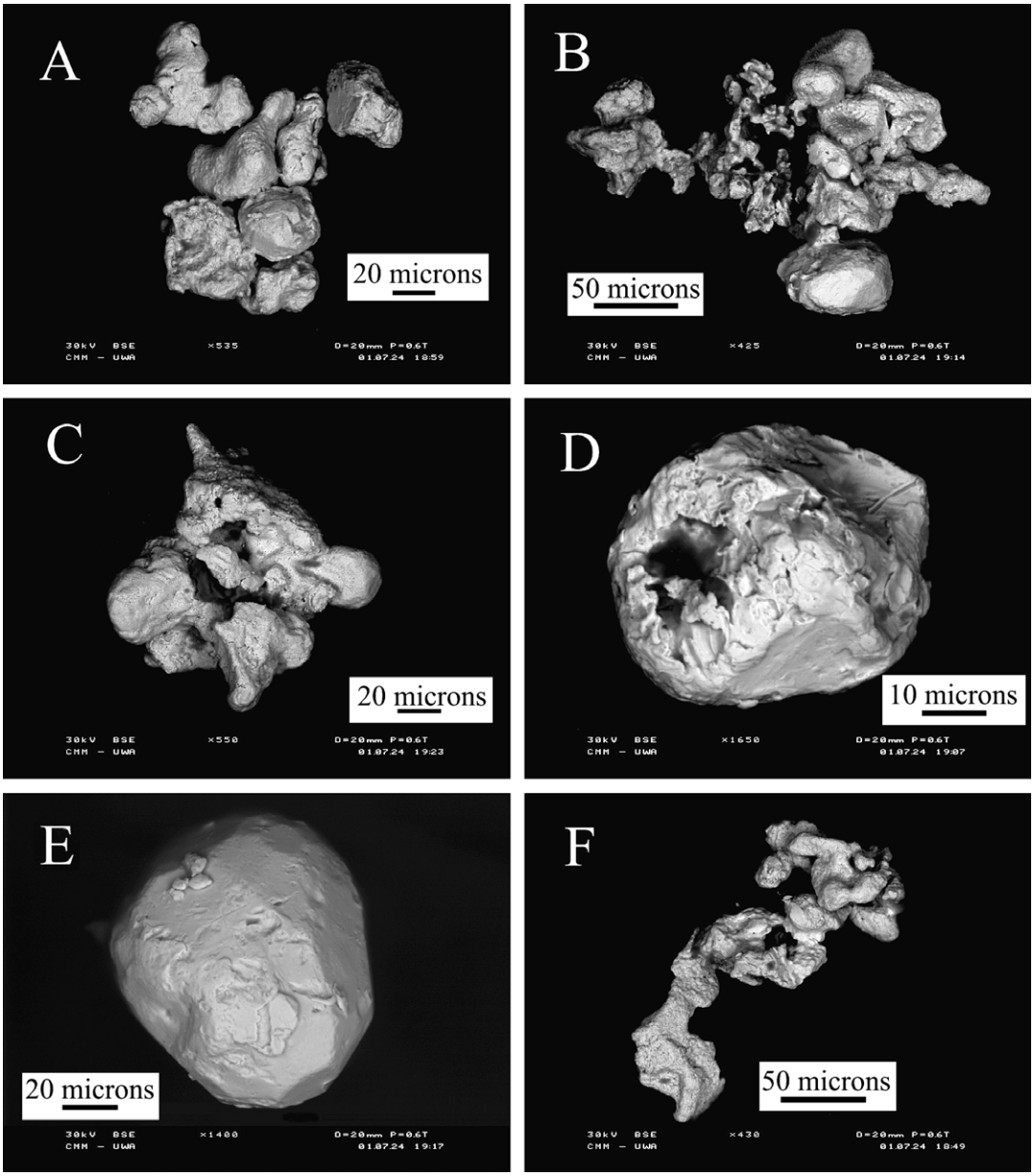

Fig. 7. Backscattered electron images (SEM) of gold grains recovered from duricrust. (A–D) Irregular particles; (E) prismatic particle; and (F) dendritic particle.

(Fig. 10, Table 4), with minor variation in Au–Ag contents within the same grain (exception for one gold grain collected in primary ore that shows variation of 6.94% Au). The highest Cu contents were observed in gold grains recovered from the fresh ore; high Ag contents are concentrated in yellow latosol grains; and high gold content is concentrated in duricrust grains (Fig. 11). These differences in composition between horizons may be a function of low, non-representative number of samples.

4.6.2. Zoned grains

Zoned grains are present throughout the regolith, and 37 of them were analysed by EMPA (Tables 2 and 3). Fig. 12A and B show the histograms of EMPA analyses for all zoned gold grains; the composition of rims and cores can be observed in black. Rims are composed of silver-poor gold (mean 3.64% Ag) and tend to be thinner in the latosol horizons. Composition of cores is bimodal, with cores containing less silver (mean 9.76% Ag) or more silver (mean 22.60% Ag). Due to the small number of grains analysed, it is not possible to correlate core and rim composition. Copper contents are similar to those in homogeneous grains. Grain cores contain <0.02–0.1% Cu in most horizons, possibly richer (>0.04–0.09% Cu) in the granophyre saprolite and poorer (<0.04% Cu) in the transition zone. Rims have a similar range of compositions (<0.02–0.15% Cu) in all horizons, except the stockwork (0.23–0.30% Cu).

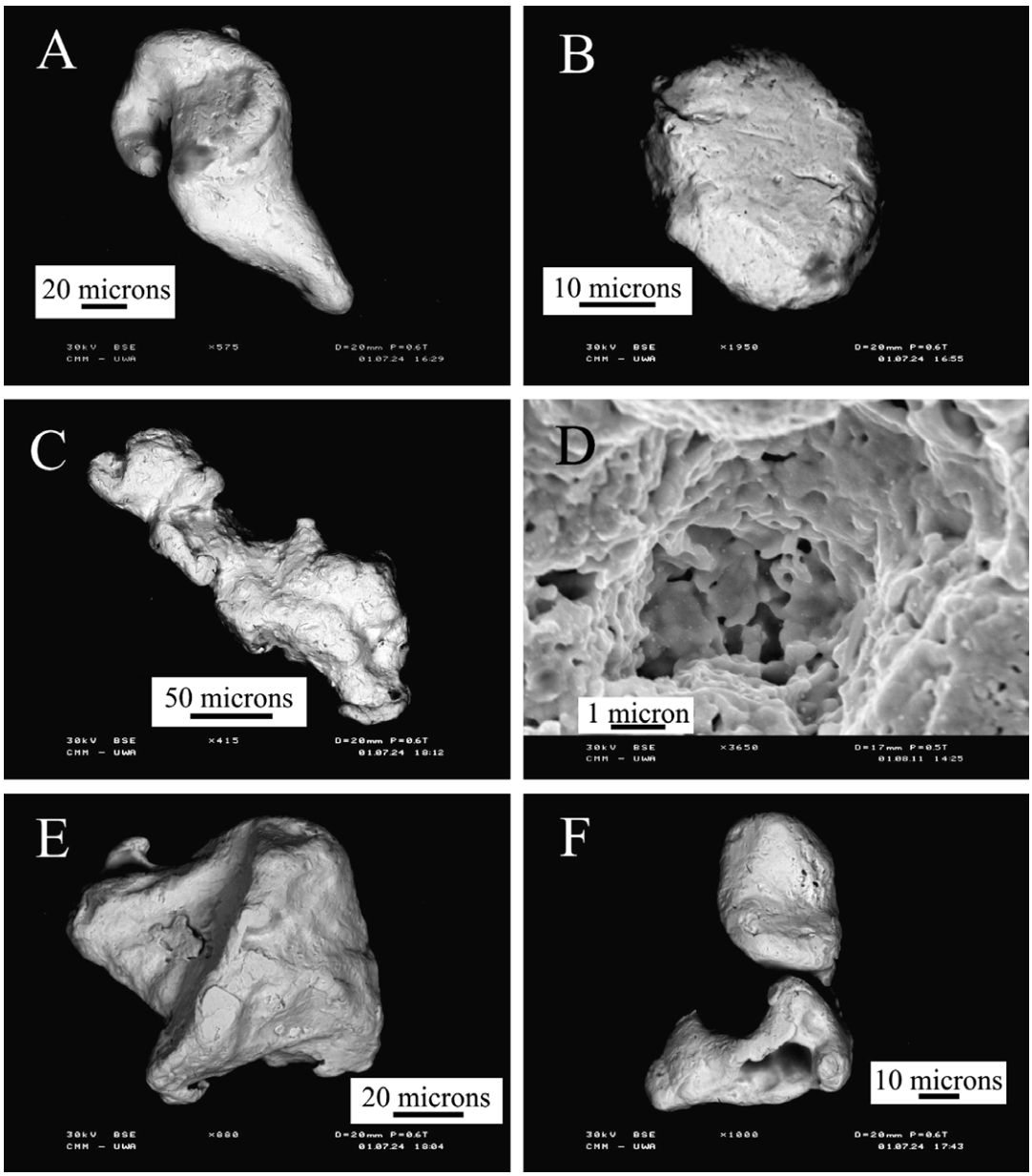

Fig. 8. Backscattered electron images (SEM) of gold grains recovered from latosols. (A–B) Particles from the red latosol, very rounded and subrounded, respectively; (C–F) particles from yellow latosol, (D) is a detail from (C).

Some zoned grains show a thin, silver-enriched zone between the core and rim and in discontinuities within a single grain (Fig. 13).

5. Discussion and conclusions

Particulate gold in the Fazenda Pison Garimpo is associated with quartz veins, situated in voids between quartz grains, and enclosed by or filling fractures in pyrite. Gold is also heterogeneously disseminated in the granophyre, stockwork zone, and quartz-rich zone. A lateritic profile composed of saprolite, transition zone, duricrust, red latosol, and yellow latosol results from the weathering evolution of underlying mineralized granophyric rock.

Gold grain sizes range from <20 to >120 μm. Primary grains are xenomorphic and irregularly distributed in the mineralized zone; gold grains are irregular, dendritic or prismatic in shape, and show smooth faces and sharp edges. The effects of weathering are visible from the base of the saprolite upward, with grains edges becoming rounded and corrosion pits evident on grain surfaces. Rounding increases slightly in the horizons of the base of the profile and abruptly from duricrust to latosol. Tool marks and folded edges likely are products of crushing and panning processes; these features are found only in some of the studied gold grains and not as a general rule.

The degrees of rounding and pitting are not homogeneous in gold grains, even those collected in the same

Table 3
Results of EMPA analyses of gold grains in polished sections

Particle	Composition	Au (%)	Ag (%)	Cu (%)
YL1	Homogeous	88.52	11.95	0.03
YL1	Homogeous	89.00	11.80	0.01
YL1	Homogeous	88.10	12.20	0.05
YL1	Homogeous	87.37	11.83	0.02
YL1	Homogeous	88.25	12.27	0.03
YL2	Homogeous	82.90	17.34	0.06
YL3	Homogeous	86.44	13.96	0.07
YL3	Homogeous	87.46	12.82	0.04
YL3	Homogeous	86.80	13.07	0.04
YL3	Homogeous	86.50	14.10	0.03
YL3	Homogeous	86.64	13.04	0.08
YL4	Zoned – rim	93.70	5.16	0.13
YL5	Zoned – rim	88.60	12.06	0.06
YL6	Zoned – rim	100.00	0.35	0.04
YL6	Zoned – rim	99.70	1.02	0.06
YL6	Zoned – rim	99.00	0.18	0.04
YL7	Zoned – rim	99.60	0.85	0.01
YL8	Zoned – rim	97.15	2.56	0.06
YL9	Zoned – rim	97.60	2.51	0.05
YL10	Zoned – rim	85.75	14.09	0.03
YL4	Zoned – core	92.36	7.40	0.10
YL5	Zoned – core	85.75	14.09	0.03
YL6	Zoned – core	77.94	21.21	0.05
YL7	Zoned – core	75.06	25.57	0.01
YL8	Zoned – core	73.34	26.87	0.04
YL8	Zoned – core	73.47	26.11	0.05
YL9	Zoned – core	74.36	24.42	0.03
YL9	Zoned – core	73.94	25.23	0.05
YL9	Zoned – core	74.56	24.68	0.03
YL9	Zoned – core	73.96	24.61	0.05
YL9	Zoned – core	74.67	24.49	0.04
YL9	Zoned – core	73.47	26.11	0.05
YL10	Zoned – core	71.25	28.64	0.07
RL1	Homogeous	91.99	7.52	0.08
RL1	Homogeous	92.90	7.40	0.05
RL1	Homogeous	91.66	7.60	0.09
RL1	Homogeous	92.07	7.61	0.08
RL2	Homogeous	91.76	8.20	0.03
RL2	Homogeous	91.72	8.21	0.05
RL3	Homogeous	90.36	9.74	0.07
RL3	Homogeous	90.07	9.56	0.13
RL3	Homogeous	90.17	9.24	0.07
RL3	Homogeous	91.20	8.78	0.05
RL3	Homogeous	91.10	8.09	0.06
RL3	Homogeous	90.96	8.53	0.05
RL4	Homogeous	89.53	9.77	0.09
RL4	Homogeous	88.83	10.80	0.09
RL4	Homogeous	88.03	11.79	0.10
RL5	Zoned – rim	92.18	7.76	0.05
RL5	Zoned – rim	98.40	0.32	0.09
RL5	Zoned – core	75.25	25.10	0.07
D1	Homogeous	97.80	2.69	0.14
D1	Homogeous	98.20	2.40	0.12
D1	Homogeous	97.65	2.43	0.12
D1	Homogeous	97.50	2.43	0.13
D2	Homogeous	96.90	3.32	0.12
D2	Homogeous	97.00	3.26	0.09
D2	Homogeous	96.48	3.22	0.14
D2	Homogeous	97.00	3.29	0.12
D2	Homogeous	96.90	3.26	0.12
D3	Homogeous	96.69	3.82	0.05
D3	Homogeous	96.13	2.59	0.20
D4	Homogeous	95.69	4.63	0.15
D4	Homogeous	95.95	4.36	0.07
D4	Homogeous	95.68	4.50	0.06
D4	Homogeous	95.50	4.49	0.06
D5	Homogeous	90.47	9.66	0.08
D6	Homogeous	95.63	4.18	0.13
D6	Homogeous	93.11	5.95	0.08
D6	Homogeous	95.19	5.55	0.10
D6	Homogeous	94.88	5.22	0.08
D6	Homogeous	95.52	5.23	0.09
D7	Zoned – rim	96.30	3.75	0.08
D7	Zoned – rim	96.50	3.64	0.02
D7	Zoned – rim	96.30	3.61	0.09
D8	Zoned – rim	93.58	6.92	0.09
D8	Zoned – rim	93.52	7.14	0.13
D9	Zoned – rim	94.12	5.92	0.09
D9	Zoned – rim	95.20	4.84	0.02
D9	Zoned – rim	95.31	5.18	0.21
D10	Zoned – rim	96.40	3.73	0.02
D10	Zoned – rim	96.96	3.84	0.03
D11	Zoned – rim	97.60	2.37	0.04
D11	Zoned – rim	90.28	10.19	0.05
D12	Zoned – rim	99.70	0.69	0.04
D12	Zoned – rim	100.00	0.16	0.03
D13	Zoned – rim	100.00	0.29	0.03
D13	Zoned – rim	100.20	0.22	0.05
D14	Zoned – rim	100.30	0.15	0.07
D14	Zoned – rim	100.30	0.07	0.03
D7	Zoned – core	89.42	9.74	0.06
D7	Zoned – core	90.60	9.29	0.05
D7	Zoned – core	85.52	14.31	0.08
D7	Zoned – core	87.07	13.14	0.07
D8	Zoned – core	89.95	9.89	0.07
D8	Zoned – core	90.34	10.15	0.04
D8	Zoned – core	90.27	9.74	0.05
D8	Zoned – core	90.82	9.78	0.04
D8	Zoned – core	77.66	23.10	0.03
D8	Zoned – core	76.88	23.49	0.03
D8	Zoned – core	77.51	23.35	0.04
D9	Zoned – core	75.52	23.58	0.01
D9	Zoned – core	78.63	21.66	0.05
D9	Zoned – core	79.59	21.04	0.03
D9	Zoned – core	77.03	23.15	0.06
D9	Zoned – core	77.56	22.56	0.04
D10	Zoned – core	87.54	12.98	0.05
D10	Zoned – core	86.96	13.68	0.13
D10	Zoned – core	88.84	11.60	0.05
D10	Zoned – core	88.38	12.21	0.07
D11	Zoned – core	78.77	21.61	0.02
D11	Zoned – core	78.10	20.74	0.05
D11	Zoned – core	80.73	20.11	0.05
D12	Zoned – core	76.59	24.08	0.05
D12	Zoned – core	90.46	9.33	0.04
D12	Zoned – core	88.95	11.02	0.05
D13	Zoned – core	78.18	21.70	0.01
D13	Zoned – core	78.66	21.89	0.01
D13	Zoned – core	78.72	21.93	0.01
D13	Zoned – core	78.84	21.20	0.02
D13	Zoned – core	70.15	30.33	0.02
D13	Zoned – core	88.92	11.76	0.08
D13	Zoned – core	87.36	12.96	0.09
D14	Zoned – core	89.88	10.19	0.10
D14	Zoned – core	91.91	8.23	0.07
D14	Zoned – core	91.98	7.76	0.05
D14	Zoned – core	90.35	9.71	0.06
TZ1	Zoned – rim	92.01	8.62	0.02
TZ2	Zoned – rim	91.48	9.08	0.05

(continued on next page)

Table 3 (*continued*)

Particle	Composition	Au (%)	Ag (%)	Cu (%)
D14	Zoned – core	87.38	12.61	0.06
TZ3	Zoned – rim	92.29	8.36	0.10
TZ4	Zoned – rim	91.05	8.78	0.04
TZ1	Zoned – core	87.72	13.00	0.01
TZ2	Zoned – core	78.60	21.23	0.02
TZ2	Zoned – core	79.08	19.90	0.01
TZ2	Zoned – core	79.15	20.81	0.04
TZ3	Zoned – core	80.07	20.63	0.03
TZ3	Zoned – core	80.62	19.24	0.02
TZ4	Zoned – core	79.23	20.34	0.01
TZ4	Zoned – core	79.15	20.32	0.01
TZ4	Zoned – core	79.30	20.69	0.01
TZ4	Zoned – core	79.11	20.76	0.03
TZ4	Zoned – core	79.19	20.46	0.04
TZ4	Zoned – core	79.02	20.64	0.01
TZ4	Zoned – core	79.37	20.45	0.03
TZ4	Zoned – core	79.46	20.20	0.05
TZ4	Zoned – core	79.30	21.00	0.01
TZ5	Zoned – core	79.97	20.74	0.01
TZ5	Zoned – core	79.68	20.29	0.08
TZ5	Zoned – core	79.70	20.84	0.01
TZ5	Zoned – core	79.67	20.70	0.01
TZ5	Zoned – core	79.02	20.64	0.01
TZ5	Zoned – core	79.37	20.45	0.03
TZ5	Zoned – core	79.46	20.20	0.05
TZ5	Zoned – core	79.30	21.00	0.01
SZ1	Zoned – rim	93.43	5.71	0.29
SZ1	Zoned – rim	94.22	5.61	0.29
SZ2	Zoned – rim	93.94	5.55	0.24
SZ2	Zoned – rim	93.71	6.00	0.23
SZ3	Zoned – rim	93.12	5.70	0.24
SZ4	Zoned – rim	94.92	5.43	0.23
SZ5	Zoned – rim	92.40	7.52	0.05
SZ1	Zoned – core	74.99	24.12	0.01
SZ1	Zoned – core	76.34	23.91	0.02
SZ1	Zoned – core	76.26	23.50	0.04
SZ2	Zoned – core	76.07	23.97	0.03
SZ2	Zoned – core	75.65	23.83	0.03
SZ3	Zoned – core	76.78	23.76	0.02
SZ3	Zoned – core	77.47	23.16	0.04
SZ4	Zoned – core	82.95	16.70	0.12
SZ5	Zoned – core	89.39	11.04	0.02
SZ5	Zoned – core	87.98	12.00	0.05
G1	Zoned – rim	94.85	5.82	0.04
G3	Zoned – rim	100.26	0.02	0.04
G4	Zoned – rim	100.74	0.02	0.05
G4	Zoned – rim	100.48	0.02	0.07
G5	Zoned – rim	100.45	0.02	0.08
G5	Zoned – rim	100.01	0.82	0.09
G6	Zoned – rim	98.96	1.02	0.15
G6	Zoned – rim	99.53	0.61	0.07
G7	Zoned – rim	99.89	0.16	0.09
G7	Zoned – rim	100.02	0.06	0.08
G7	Zoned – rim	100.04	0.02	0.04
G8	Zoned – rim	98.92	1.30	0.04
G8	Zoned – rim	99.04	0.44	0.05
G9	Zoned – rim	99.85	0.23	0.01
G1	Zoned – core	68.35	31.10	0.07
G2	Zoned – core	75.07	24.70	0.09
G3	Zoned – core	86.07	13.03	0.15
G4	Zoned – core	88.03	11.79	0.07
G4	Zoned – core	88.48	10.55	0.09
G4	Zoned – core	89.59	10.86	0.08
G5	Zoned – core	90.30	9.99	0.08
G5	Zoned – core	90.15	10.58	0.09

Table 3 (*continued*)

Particle	Composition	Au (%)	Ag (%)	Cu (%)
G6	Zoned – core	92.54	7.62	0.08
G6	Zoned – core	92.19	7.34	0.08
G6	Zoned – core	92.21	7.66	0.09
G6	Zoned – core	92.56	7.27	0.07
G7	Zoned – core	94.76	5.28	0.07
G7	Zoned – core	94.98	4.94	0.04
G7	Zoned – core	94.70	5.34	0.04
G8	Zoned – core	95.68	4.79	0.09
G8	Zoned – core	96.28	4.29	0.07
G8	Zoned – core	96.08	3.84	0.08
G9	Zoned – core	93.68	7.05	0.05
FO1	Homogeous	91.80	7.65	0.05
FO1	Homogeous	91.27	8.16	0.08
FO1	Homogeous	91.44	8.15	0.20
FO2	Homogeous	88.29	10.64	0.17
FO2	Homogeous	89.19	10.53	0.87
FO2	Homogeous	88.88	10.71	0.73
FO3	Homogeous	82.25	17.05	0.02
FO4	Homogeous	85.68	13.63	0.35
FO4	Homogeous	86.00	13.50	0.21
FO5	Zoned	96.30	3.49	0.19
FO5	Zoned	72.85	26.92	0.07
FO6	Zoned	96.69	3.62	0.17
FO6	Zoned	75.96	24.16	0.06

Table 4
Summary statistics report for EMPA analyses of gold grains

Variable	Count	Mean	StdDev	Min	Max	Range
Homogeneous						
Au (%)	56	91.63	4.11	82.25	98.20	15.95
Ag (%)	56	8.28	4.00	2.40	17.34	14.94
Cu (%)	56	0.12	0.15	0.01	0.87	0.86
Zoned – rim						
Au (%)	54	96.48	3.63	85.75	100.74	14.99
Ag (%)	54	3.64	3.60	0.02	14.09	14.07
Cu (%)	54	0.08	0.07	0.01	0.29	0.28
Zoned – core						
Au (%)	104	82.71	7.00	68.35	96.28	27.93
Ag (%)	104	17.30	6.91	3.84	31.10	27.26
Cu (%)	104	0.05	0.03	0.01	0.15	0.14

regolith material. This difference is caused by differential exposition to weathering solutions. Whereas some grains were totally free of surrounding primary minerals, others were partially or totally encapsulated by quartz or other minerals. Therefore, (1) in a single grain, it is possible to observe smooth surfaces and sharp edges in one area and rounded edges and corrosion pits in another; (2) gold grains show different degrees of weathering in the same regolith horizon; and (3) gold grains in upper horizons show less weathering than some of those found below in the lateritic profile. It is also possible to observe that, as a general rule, rounding and pitting increase upward in the profile, and the mean grain size decreases progressively from duricrust upward as corrosion and dissolution continue.

In the duricrust, the presence of gold particles with cores with different Ag content indicate that some aggregate grains comprising several smaller particles formed (note

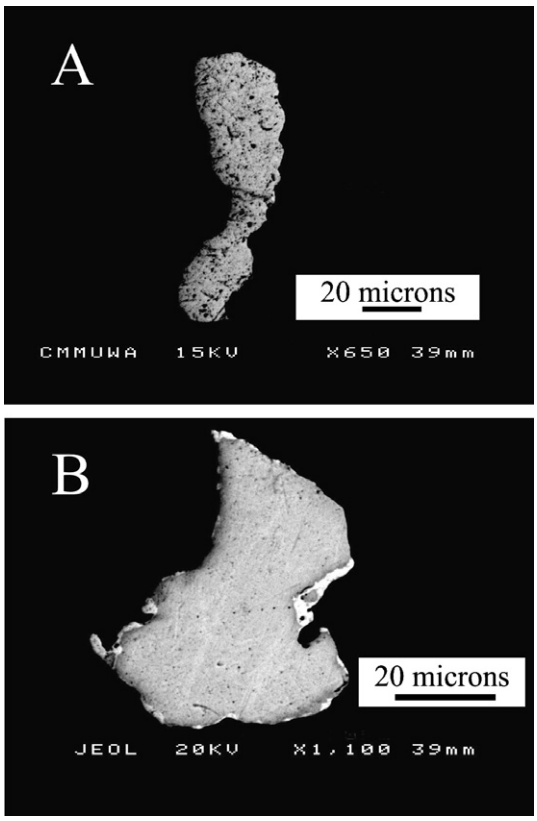

Fig. 9. Backscattered electron image (SEM) of polished sections of gold particles. (A) Homogeneous gold grain; (B) zoned gold grain.

different tones of grey in the particle shown in Fig. 14). The cores of these individual small particles have different Au/Ag compositions and were joined by zones of Ag-poor gold between them. The largest gold grains (mean 124 μm) were found in the duricrust; only smaller grains were observed in the materials present below the duricrust, which suggests that a process of gold grain development was active during iron duricrust formation. Gold nugget formation in lateritic profiles was reported previously, for example, by Machairas (1963), Mann (1984), and Wilson (1984).

These aggregates were not found in the overlying red and yellow latosols, which suggests that the process of duricrust transformation into latosol was accompanied by gold dissolution and particle division. Silver-poor rims are thinner in the latosols than in the duricrust, suggesting a progressive upward weathering in the profile. Gold grades are higher in the latosol than in the duricrust (Larizzatti, 2002), despite the smaller size and number of gold particles recovered from latosol, which also suggests gold was dissolved during the transformation of duricrust into latosol.

All gold grains observed in the regolith are interpreted as residual relicts that survived weathering of the primary mineralization. To support this hypothesis, we note (1) the mushroom-type gold anomaly observed just above mineralized quartz veins (Larizzatti, 2002); (2) that an exploration survey performed in the area (geophysics, geochemistry, drilling; RTDM, 1995) was unable to find other known mineralization in the vicinities of the studied mineralized profile; (3) the presence of relict pisoliths of iron oxihydroxides (fragments of duricrust) in the latosol (Larizzatti, 2002); and (4) the recognition, despite weathering processes, of gold grain primary habits, similar to those observed in the saprolite, in the latosols.

Grains of weathered primary gold with Ag-poor rims and Ag-rich zones on internal grain boundaries have also been observed at Gentio do Ouro in the semiarid northeast of Brazil (Grimm and Friedrich, 1990) and have several features similar to those seen at Fazenda Pison. Silver enrichment always occurs at the contact between the primary core of the grain and the Ag-depleted rim or zone, and there is an abrupt contact between silver-rich zones and silver-poor rims. However, at Fazenda Pison, the contacts between the Ag-rich zones and the core of primary gold grains tend to be gradational, as shown in Fig. 14A and B. Grimm and Friedrich (1990) suggest Ag-rich zones "result from mobilization, separation, and rapid precipitation of electrum by thiosulphate complex formation" during weathering.

Webster and Mann (1984) stress the influence of climate, rock composition, and geomorphological factors in gold mobility. The supergene conditions prevailing in the Amazon (one bar atmospheric pressure; temperatures of 20–30 °C; excess free water), the presence of pyrite in the primary ore, the abundance of organic matter in the surface soil, and the mushroom-shaped surface dispersion pattern of gold at Fazenda Pison (Larizzatti, 2002) suggest the metal could be complexed by a wide range of ligands and is relatively soluble (Goleva, 1970; Roslyakov et al., 1971; Baker, 1978; Plyusnin et al., 1981; Stoffregen, 1986; Webster, 1986; Vlassopoulos and Wood, 1990; Bowell, 1993).

Evidence of gold dissolution includes the progressive decrease in grain size upward in the lateritic profile (except in the duricrust, where grains are aggregates of separate individual small grains) and the presence of corrosion features on grain surfaces, as observed by other authors (Colin et al., 1989a,b; Colin and Vieillard, 1991; Porto and Hale, 1996). Rounding and pitting increase upward in the profile, indicating dissolution of gold due to exposure to weathering solutions. There is, however, no unequivocal evidence of reprecipitation of secondary gold. In most weathering environments, secondary gold is of very high fineness, containing less than 1.0% Ag (e.g., Mann, 1984; Butt, 1989; Freyssinet et al., 1987; Santosh and Omana, 1991; Gray et al., 1992). All gold recovered at Fazenda Pison contain silver, either throughout in homogeneous grains or in the core in zoned grains; even the rims of most zoned grains contain >1.0% Ag. No grains of pure gold were recovered, though this may be a function of sample preparation, in that few grains <10 μm were recovered. The secondary gold noted by Freyssinet et al. (1987) in Mali, for example, is very fine grained, mostly <1 μm, and fragile dendrites, readily destroyed by panning. Freyssinet et al. (1987) and Santosh and Omana (1991) also observe fine secondary grains in cavities in gold grains, but these were not found at Fazenda Pison.

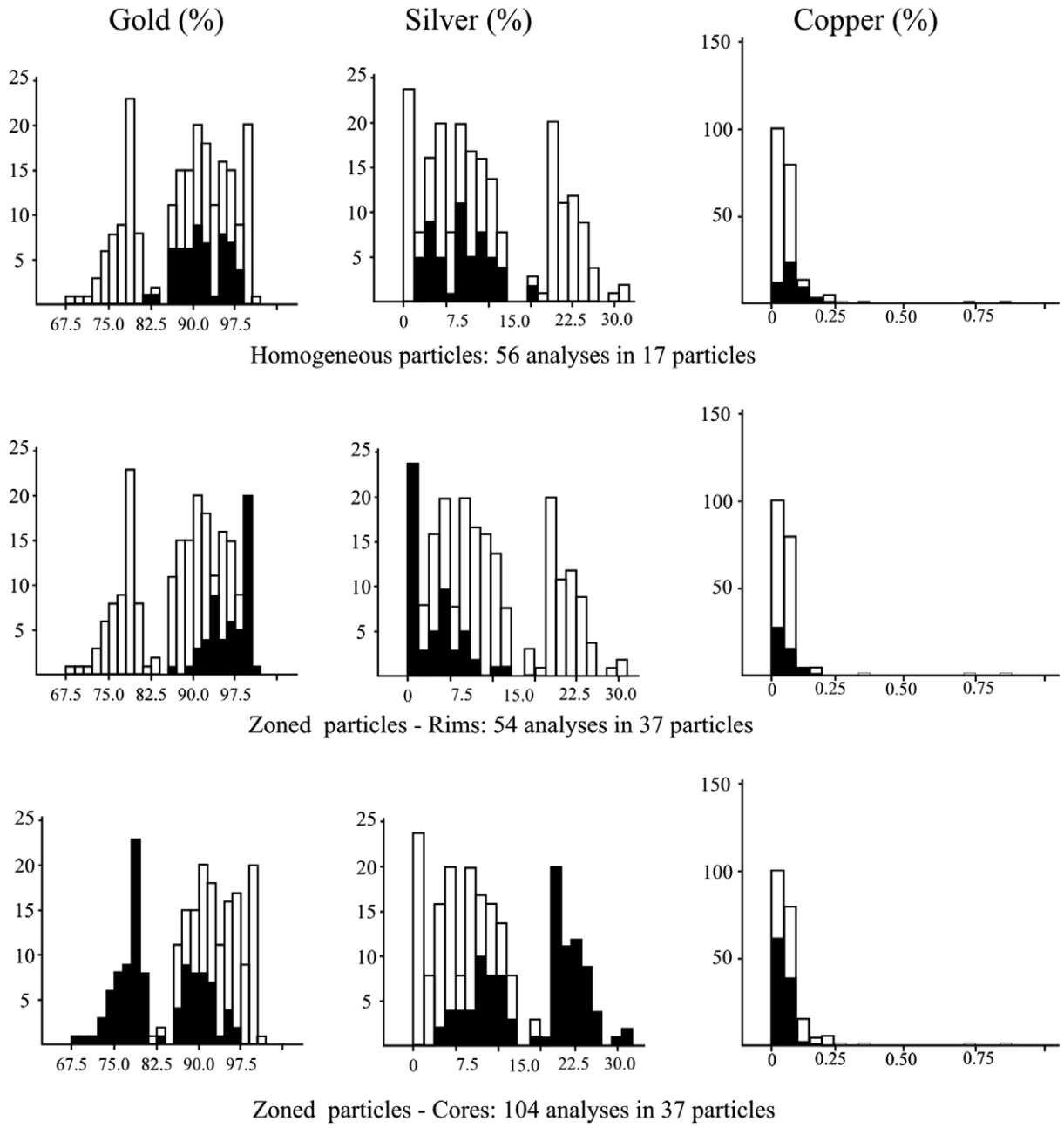

Fig. 10. Frequency diagrams for "N" analyses of Au, Ag, and Cu contents in 17 homogeneous gold particles and 37 zoned gold particles. All data shown in outline, with results for each phase highlighted in black. (EPMA analyses.)

Silver (0.1–25%) and trace copper (0.02–0.9%) are the only elements other than gold present in significant abundance. Compositions generally vary from grain to grain or even within the same grain, as noted by other authors (e.g., Boyle, 1979; Desborough et al., 1971; Antweiler and Campbell, 1977; Morrison et al., 1991; Knight et al., 1999). The grains are either homogeneous (with minor variations in Au–Ag contents) or zoned, with silver-rich cores and thin, silver-poor rims. Some of these silver-poor rims are composed of essentially pure gold. Copper contents show much less variation, with similar abundances in homogeneous grains, cores, and rims. Gold from the stockwork saprolite differs from that in the granophyre saprolite, in that both cores and rims in grains from the stockwork appear to be more silver rich, and rims are relatively rich in copper.

Silver-poor rims have been observed on the surfaces of primary gold grains in lateritic profiles and placer deposits (Desborough, 1970; Mann, 1984; Giusti, 1986; Michel, 1987; Freyssinet et al., 1987; Freyssinet and Butt, 1988). The presence of zoned grains in the regolith at Fazenda Pison, silver-poor zones adjacent to internal fractures and as rims to the grains, sharp internal contact between the core and these zones, and high fineness of the rims are

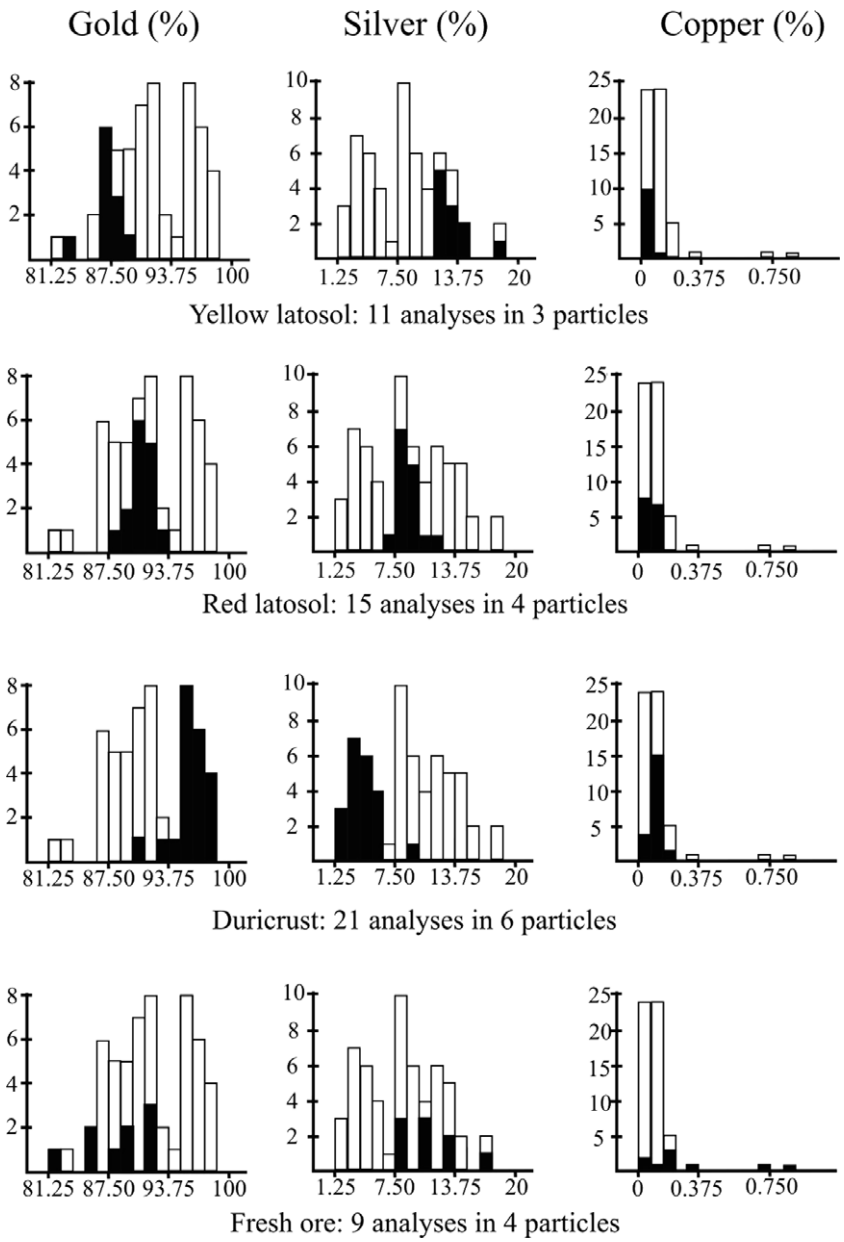

Fig. 11. Frequency diagrams for "N" analyses of Au, Ag, and Cu contents in 17 homogeneous gold particles. All data shown in outline, with results for each phase highlighted in black. (EPMA analyses.)

consistent with the rims being secondary features. The results from Fazenda Pison provide more quantitative data for silver and copper, which indicate a general relationship between the silver contents of core and rim and that copper contents are seemingly unchanged. These latter observations differ from other reports, which do not note any compositional relationships between core and rim, rather the absence of both silver and copper. The presence of zones of silver enrichment between the rim and core confirms similar findings by Grimm and Friedrich (1990). Three principal theories can be advanced regarding the formation of silver-poor rims:

1. *Precipitation (plating) of gold.* The Ag-poor gold is derived from higher levels in the regolith profile, toposequence or drainage, and precipitates on the surface of the grain. Precipitation can be caused by changes in solution chemistry, reaction with metal ions such as Fe and Mn that break down complexing ligands (Conklin and Hoffmann, 1988), or catalysis by solids (Boyle, 1979), of which free gold is one of the most effective. Plating by reprecipitated gold is considered to have occurred in some placer deposits, which may contain pristine, commonly fragile, discrete grains of secondary gold, and zoned grains in which relict primary gold has silver-poor rims exhibiting delicate structures and clear crystalline habits (e.g., Webster and Mann, 1984; Giusti, 1986; McCready et al., 2003). Such structures have not been reported from weathering profiles; crystalline and other forms of secondary gold are described as dis-

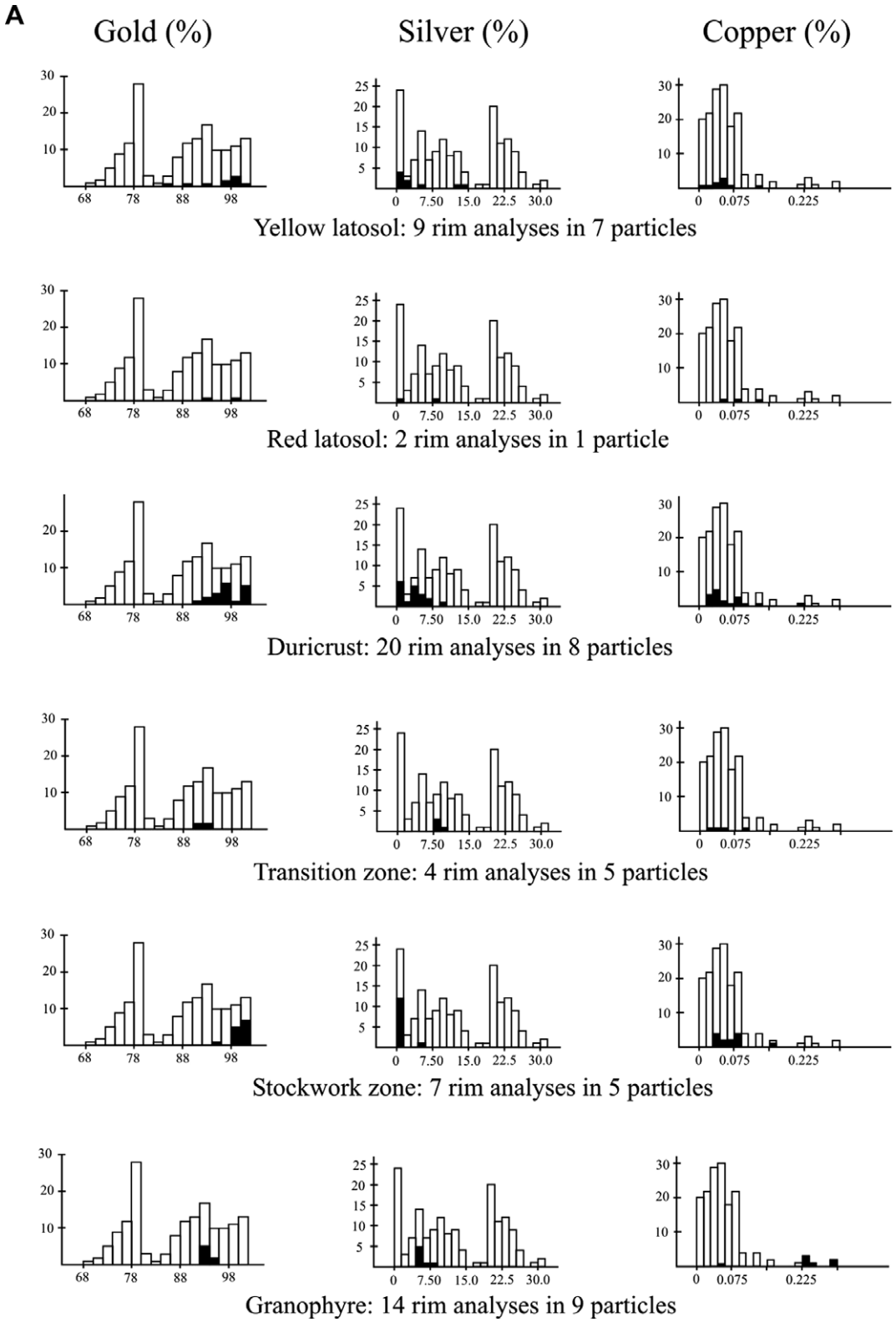

Fig. 12. Frequency diagrams for "N" analyses of Au, Ag, and Cu contents in (A) rims and (B) cores of 37 zoned particles. All data shown in outline, with results for each phase highlighted in black. (EPMA.)

crete grains, not continuous overgrowths on relict primary grains. Furthermore, precipitation along internal discontinuities is difficult to explain by this mechanism.

2. *Self-electrorefining.* In this process, an Au–Ag alloy dissolves electrochemically at the interface with a weathering solution, and gold, the more inert metal, reprecipitates

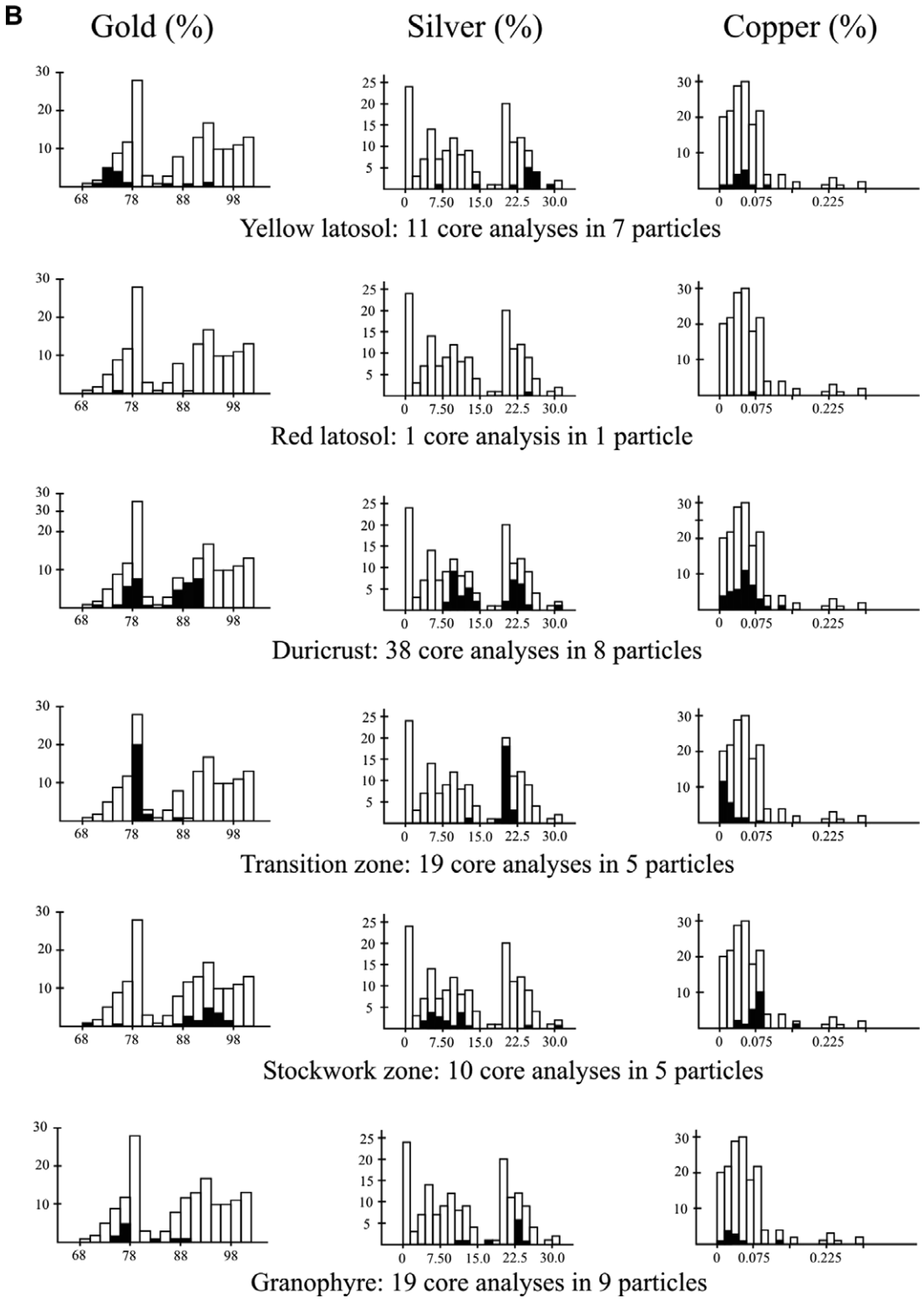

Fig 12. (*continued*)

onto the surface of the grain (Groen et al., 1990). The process results in the formation of lobate overgrowths of reprecipitated Au, and silver is leached by the weathering solution. The reaction is maintained by the difference in electrical potential between the gold-rich areas and the primary gold–silver alloy. However, overgrowths that completely cover the primary grain core would restrict access to the primary gold–silver alloy and interrupt the process.

3. *Selective depletion of silver.* Preferential silver depletion from the primary grain by interaction with soil,

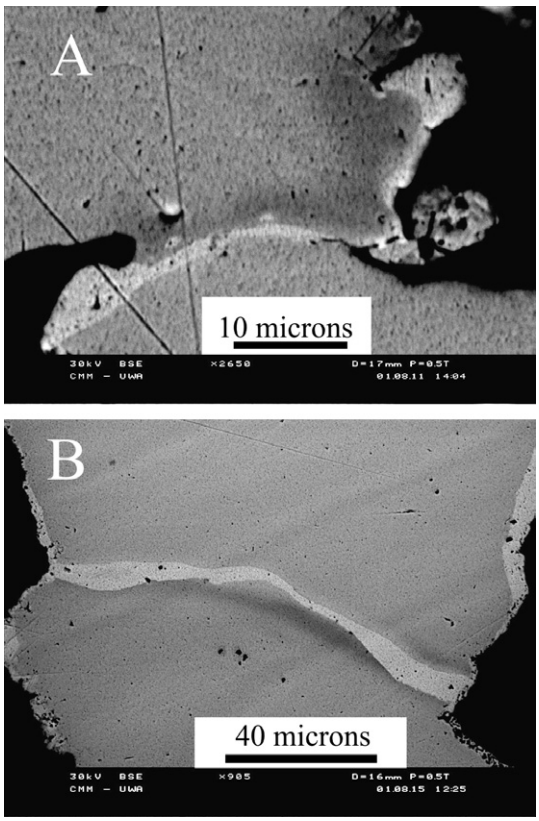

Fig. 13. SEM images (backscattered electrons) of gold grains recovered from saprolite (granophyre) showing silver-enriched zones (dark grey), following discontinuities in gold grains filled by silver-poor gold (light grey).

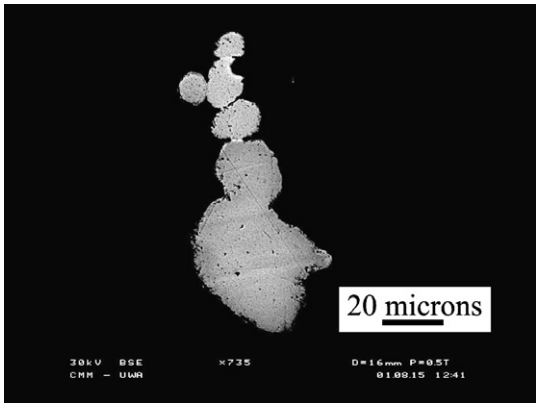

Fig. 14. Backscattered electron image (SEM) of a zoned aggregate grain from duricrust, with silver-poor zones at the contact between individual particles. Note different tones of grey in core zones.

ground, or drainage water is the most probable process in the regolith, with the presence of silver-poor zones along internal fractures as the most compelling evidence (Colin and Vieillard, 1991; Gray et al., 1992). Silver depletion develops from the outer rims and discontinuities (probably crystal boundaries) within the grains, allowing weathering solutions to interact from the surface to the centre of the grains. According to Gray et al. (1992), the rims could be a consequence of galvanic reactions on the grain surface involving simultaneous solution of Ag^{+} and Au^{+} ions. Gold would reprecipitate immediately, whereas Ag would be removed by the leaching solution. Retention of Cu in the rims and zones of silver enrichment, noted in this study, add weight to this conclusion.

The variations in morphology and composition of gold grains in the regolith at the Fazenda Pison "Garimpo" are products of processes that have caused the weathering of the mineralized rocks to form saprolite, the formation of the lateritic duricrust, the destruction of the duricrust, and its transformation to latosol. Costa (1997) describes mature and immature laterite profiles in the Amazon region as a result of two distinct periods of laterite formation in different climatic conditions. The observation that large, aggregate grains occur only in the duricrust may be significant, assuming it is not due to poor sampling statistics or a variation in the primary mineralization. It is possible these are remnants of primary polycrystalline grains, preserved by the cementation of the duricrust. Similar grains would have been present in the saprolite, but ongoing exposure to weathering may have caused them to disaggregate or be sufficiently weakened not to survive panning. Similarly, aggregates released from duricrust during latosol formation may have been further weathered, so that none survived. The corrosion of silver-poor rims on grains in the latosol is evidence for this latter weathering.

Acknowledgments

This research was undertaken as part of a Ph.D. research project by JHL at the University of Sao Paulo and during a study visit to the CRC for Landscape Evolution and Mineral Exploration, CSIRO Division of Exploration and Mining, and the University of Western Australia in Perth, Western Australia. FAPESP (State of São Paulo Research Foundation) is acknowledged for research Grant 1999/1537-9. CAPES Foundation (Coordination of Training of Higher Education Graduate) is acknowledged for scholarship BEX0575/00-3. Prof. Dr. Rômulo Angélica is thanked for discussions on gold grain geochemistry and morphology and for his suggestions and comments as a reviewer. Dr. Erik Van Noort is thanked for discussions during EMPA analysis. Prof. Dr. Brendan J. Griffin and Ms. Sharon Platten are thanked for SEM assistance. Dr. Robert Hough is thanked for comments on a previous version of the manuscript. Constructive reviews by Dr. J.C. Parisot helped improve the manuscript.

References

de Almeida, F.F.M., Hasui, Y., de Brito Neves, B.B., Fuck (sic), R.A.A., 1981. Brazilian structural provinces: an introduction. Earth Science Review 17, 1–29.

Andrade, A.F., Santiago, A.F., Melo, C.F., Bizinella, G.A., Moreira, H.L., Santos, J.O.S., Oliveira, J.R., Moura, P.A., Lopes, R.C., Rosa Filho, S.F., Neves, S.A.V., 1978. Projeto Tapajós – Sucunduri: relatório de integração geolóaus, CPRM/DNPM. 3v. (internal report).

Andrade, W.O., Mackesky, M.L., Rose, A.W., 1991. Gold distribution and mobility in the surficial environment, Carajás region, Brazil. Journal of Geochemical Exploration 40, 95–114.

Angélica, R.S., Costa, M.L., Pöllmann, H., 1995. Mineralogia e geoquímica das partículas de ouro nos perfis laterito-gossânicos das áreas Igarapé Bahia e Águas Claras, Carajás, Pará. In: V Congr. Bras. Geoq., Anais, Niterói, RJ.

Antweiler, J.C., Campbell, W.L., 1977. Application of gold compositional analyses to mineral exploration in the United States. Journal of Geochemical Exploration 8, 17–29.

Baker, W.E., 1978. The role of humic acid in the transport of gold. Geochimica et Cosmochimica Acta 42, 645–649.

Bowell, R.J., 1992. Supergene gold mineralogy at Ashanti, Ghana: implications for the supergene behavior of gold. Mineralogical Magazine 56, 545–560.

Bowell, R.J., 1993. The role of fulvic acid in the supergene migration of gold in tropical rain forest soils. Geochimica et Cosmochimica Acta 57, 4179–4190.

Boyle, R.W., 1979. The geochemistry of gold and its deposits. Geological Survey of Canada Bulletin 280, 564p.

Benedetti, M., Boulège, J., 1991. Mechanism of gold transfer and deposition in a supergene environment. Geochimica et Cosmochimica Acta 55, 1539–1547.

Butt, C.R.M., 1989. Genesis of supergene gold deposits in the lateritic regolith of the yilgarn block, Western Australia. In: Keays, R.R., Ramsay W.R.H., Groves, D.I. (Eds.), The Geology of Gold Deposits: The Perspective in 1988. Economic Geology Monograph 8. Proceedings of Bicentennial Gold 88, 460–470.

Colin, F., Edou-Minko, A., Nahon, D., 1989a. Lór particulaire dans le profils latéritiques: altérations géochimiques et disprsion superficielles em cditions équatorialles. Comptes Rendues de ÍAcadémie des Sciences, Paris 309 (serie II), 553–560.

Colin, F., Lecomte, P., Boulangé, B., 1989b. Dissolution features of gold grains in a lateritic profile at Dondo Mobi, Gabon. Geoderma 45, 241–250.

Colin, F., Vieillard, P., 1991. Behavior of gold in the lateritic equatorial environment: weathering and surface dispersion of residual gold grains, at Dondo Mobi, Gabon. Applied Geochemistry 6, 279–290.

Conklin, M.H., Hoffmann, M.R., 1988. Metal ion–sulfur (IV) chemistry. 3. Thermodynamics and kinetics of transient iron (III)–sulfur (IV) complexes. Environmental Science & Technology 22, 899–907.

Costa, M.L., 1997. Lateritization as a major process of ore deposit formation in the Amazon region. Exploration and Mining Geology 6, 79–104.

CPRM, 1999. Geology and Mineral Resources of Vila Mamãe Anã Sheet (SB.21-V-D). 1:250.000 scale. CPRM, Manaus, 60p, unpublished (in Portuguese).

Craw, D., 1992. Growth of alluvial gold grains by chemical accretion and reprecipitation, Waimumu, New Zealand. New Zealand Journal of Geology and Geophysics 35, 157–164.

Davy, R., El-Ansary, M., 1986. Geochemical patterns in the laterite profile at Boddington gold deposit, Western Australia. Journal of Geochemical Exploration 26, 119–144.

Desborough, G.A., 1970. Silver depletion indicated by microanalysis of gold from placer occurrence, Western United States. Economic Geology 65, 304–311.

Desborough, G.A., Heidel, R.H., Raymond, W.H., Tripp, J., 1971. Primary distribution of silver and copper in native gold from six deposits in the Western United States. Mineralium Deposita 6, 321–334.

Edou Minko, A., Colin, F., Trescases, J.J., Lecomte, P., 1992. Altération latéritique du gîte aurifère d'Ovala (Gabon), et formation d'une anomalie superficielle de dispersion. Mineralium Deposita 27, 90–100.

Eyles, N., 1990. Post-depositional gold nugget accretion in Late Cenozoic glacial placer deposits of Western Canada. Sediments 1990 – 13th International. Sedimentological Congress, pp. 74–75.

Freyssinet, P., Butt, C.R.M., 1988. Morphology and geochemistry of gold in a lateritic profile, Reedy mine, Western Australia. CSIRO Australia Division of Exploration Geoscience Restricted Report MG 58R. 15pp.

Freyssinet, P., Zeegers, H., Tardy, Y., 1987. Néoformation d'or dans les cuirrasses latéritiques, dissolution, migration, précipitation. Comptes Rendues de l' Académie des Sciences, Paris 305 (série II), 867–874.

Freyssinet, P., 1993. Gold dispersion related to ferricrete pedogenesis in South Mali: application to geochemical exploration. Chronique de. Recherche des Mines 510, 25–40.

Giusti, L., 1986. The morphology, mineralogy, and behaviour of "fine grained" gold from placer deposits of Alberta: sampling and implications for mineral exploration. Canadian Journal of Earth Sciences 23, 1662–1672.

Goleva, G.A., 1970. Geochemical trends in the occurrence and migration forms of gold in natural waters. Geochemistry International 7, 518–529.

Gray, D.J., Butt, C.R.M., Lawrance, L.M., 1992. The geochemistry of gold in lateritic terrains. In: Butt, C.R.M., Zeegers, H. (Eds.), Regolith Exploration Geochemistry in Tropical and Subtropical Terrains. Handbook of Exploration Geochemistry, 4. Elsevier, Amsterdam, pp. 461–482.

Grimm, B., Friedrich, G., 1990. Weathering effects on supergene gold in soils of a semiarid environment, Gentio do Ouro, Brazil. In: Noack, Y., Nahon, D. (Eds.), Geochemistry of the Earth's Surface and of Mineral Formation. Chemical Geology, 84, 70–73.

Groen, J.C., Craig, J.R., Rimstidt, J.D., 1990. Gold-rich rim formation on electrum grains in placers. Canadian Mineralogist 28, 207–228.

Knight, J.B., Mortensen, J.K., Morison, S.R., 1999. Lode and placer gold composition in the Klondike district, Yukon Territory Canada: implications for the nature and genesis of Klondike placer and lode gold deposits. Economic Geology 94, 649–664.

Lawrance, L.M., Griffin, B.J., 1994. Crystal features of supergene gold at Hannan South, Western Australia. Mineralium Deposita 29, 391–398.

Larizzatti, J.H., 2002. Gold and pathfinder elements in the regolith of Fazenda Pison garimpo – dispersion processes and implications for exploration. Unpublished PhD. thesis. University of São Paulo, 204p. (in Portuguese).

Machairas, G., 1963. Étude des phénomènes de migration chimique de l'or. Cas de la Guyane Française et d'Ity en Côte-d'Ivoire. Bull. Soc. Franç. Minér. Crist. 86, 78–80.

Mann, A.W., 1984. Mobility of gold and silver in lateritic weathering profiles, some observations from Western Australia. Economic Geology 79, 38–49.

Michel, D., 1987. Concentration of gold in situ laterite from Mato Grosso. Mineralium Deposita 22, 185–189.

McCready, A.J., Parnell, J., Castro, L., 2003. Crystalline placer gold from the Rio Neuquén, Argentina: implications for the gold budget in placer gold formation. Economic Geology 98, 623–633.

Morrison, G.W., Rose, W.J., Jaireth, S., 1991. Geological and geochemical controls on the silver content (fineness) of gold in gold–silver deposits. Ore Geology Reviews 6, 333–364.

de Oliveira, S.M.B., Campos, E.G., 1991. Gold-bearing iron duricrust in Central Brazil. Journal of Geochemical Exploration 41, 233–244.

de Oliveira, S.M.B., de Oliveira, N.M., 2000. The morphology of gold grains associated with oxidation of sulphide-bearing quartz veins at São Bartolomeu, central Brazil. Journal of South American Earth Sciences 13, 217–224.

Plyusnin, A.M., Pogrelniak, Y.F., Mironov, A.G., Zhmodik, S.M., 1981. The behavior of gold in the oxidation of gold bearing sulphides. Geochemistry International 18, 116–123.

Porto, C.G., Hale, M., 1996. Mineralogy, morphology and chemistry of gold in stone line lateritic profile of the Posse deposit, Central Brazil. Journal of Geochemical Exploration 57, 115–125.

RTDM, 1995. Relatório de avaliação do potencial aurífero da área Fazenda Pison (AM). Rio Tinto Denvolvimentos Minerais. Confidential report, 29pp. (in Portuguese).

Roslyakov, N.A., Peshevitsky, B.I., Nepeyna, L.A., Timbalist, V.G., 1971. Geochemistry of gold in processes of weathering crust formation. International Geological Congress, Moscow, Abstracts of reports. II, 179–180.

Santos, J.O.S., Hartman, L.A., Gaudetti, H.E., 1997. Reconnaissance U–Pb in zircon, Pb–Pb in sulphides and review of Rb–Sr geochronology in the Tapajós Gold Province, Pará/Amazonas States, Brazil. South

American Symposium on Isotope Geology – Brazil (SSAGI), Campos do jordão, SP. Proceedings. 280–282.

Santos, J.O.S., Groves, D.I., Hartmann, L.A., Moura, M.A., McNaughton, N.J., 2001. Alta Floresta Domains, Tapajós-Parima orogenic belt, Amazon Craton, Brazil. Mineralium Deposita 36, 278–299.

Santosh, M., Omana, P.K., 1991. Very high purity gold from lateritic weathering profiles of Nilambur, southern India. Geology 19, 746–749.

Sergeev, N.B., Zaikov, V.V., Laputina, L.P., Trofimov, O.V., 1994. Gold and silver in the supergene zone of the pyritic lode off the Gai deposit, the southern Urals. Geology of Ore Deposits 36, 152–164.

Stoffregen, R., 1986. Observations on the behavior of gold during supergene oxidation at Summitville, Colorado, U.S.A., and implications for electrum stability in the weathering environment. Applied Geochemistry 1, 549–558.

Vasconcelos, P.M., Kyle, J.R., 1991. Supergene geochemistry and crystal morphology of gold in a semiarid weathering environment, application to gold exploration. Journal of Geochemical Exploration 40, 115–132.

Vlassopoulos, D., Wood, S.A., 1990. Gold speciation in natural waters. I. Solubility and hydrolisis reactions of gold in aqueous solution. Geochimica et Cosmochimica Acta 54, 3–12.

Webster, J.G., Mann, A.W., 1984. The influence of climate, geomorphology and primary geology on the supergene migration of gold and silver. Journal of Geochemical Exploration 22, 21–42.

Webster, J.G., 1986. The solubility of gold and silver in the system Au–Ag–S–O_2–H_2 at 25 °C and 1 atm. Geochimica et Cosmochimica Acta 50, 1837–1846.

Wilson, A.F., 1984. Origin of quartz-free gold nuggets and supergene gold found in laterites and soils – a review and some new observations. Australian Journal of Earth Sciences 31, 303–316.

Youngson, J.H., Craw, D., 1995. Evolution of placer gold deposits during regional uplift, Central Ontago, New Zealand. Economic Geology 90, 731–745.

Zang, W., Fyfe, W.S., 1993. A three-stage genetic model for the Igarapé Bahia lateritic gold deposit, Carajás, Brazil. Economic Geology 88, 1768–1779.